catalysts

MDPI

Article

Efficiency of Microwave-Assisted Surface Grafting of Ni and Zn Clusters on TiO_2 as Cocatalysts for Solar Light Degradation of Cyanotoxins

Andraž Šuligoj [1,2,*], Mallikarjuna Nadagouda [3], Gregor Žerjav [1], Albin Pintar [1], Dionysios D. Dionysiou [4,†] and Nataša Novak Tušar [1,5]

[1] Department of Inorganic Chemistry and Technology, National Institute of Chemistry, Hajdrihova 19, SI-1000 Ljubljana, Slovenia; gregor.zerjav@ki.si (G.Ž.); albin.pintar@ki.si (A.P.); natasa.novak.tusar@ki.si (N.N.T.)
[2] Faculty of Chemistry and Chemical Technology, University of Ljubljana, Večna pot 113, SI-1000 Ljubljana, Slovenia
[3] Department of Mechanical and Materials Engineering, Wright State University, Dayton, OH 45435, USA; nadagouda.mallikarjuna@epa.gov
[4] Environmental Engineering and Science Program, Department of Chemical and Environmental Engineering (ChEE), University of Cincinnati, Cincinnati, OH 45221, USA
[5] Graduate School, University of Nova Gorica, Vipavska 13, 5000 Nova Gorica, Slovenia
* Correspondence: andraz.suligoj@ki.si
† Deceased author.

Abstract: Herein, we report on the synthesis of Ni and Zn clusters on the surface of TiO_2 as well as their bimetallic NiZn analogs. The materials were prepared by incipient wet impregnation of colloidal TiO_2 followed by microwave (MW) irradiation to graft the clusters to TiO_2 surface. The materials were further immobilized onto glass slides and exhibited high surface area, high mechanical stability, and porosity with accessible pores. The main species responsible for visible light degradation of microcystin LR via the interface charge transfer (IFCT) of excited e^- to surface metal clusters were found to be $O_2^{\bullet -}$ and h^+. The optimal nominal grafting concentration was 0.5 wt.% for Ni and 1.0 wt.% for Zn, while for the bimetal modification (NiZn), the optimal nominal concentration was 0.5 wt.%. Compared to monometallic, bimetallic grafting showed a lower kinetic constant, albeit still improved compared to bare TiO_2. Bimetal-modified titania showed a lower photocurrent compared to single metal-grafted TiO_2 and poorer interfacial charge transport, namely, more recombination sites—possibly at the interface between the Ni and Zn domains. This work highlights the efficiency of using MW irradiation for grafting sub-nano-sized metallic species to TiO_2 in a homogeneous way. However, further strategies using MW irradiation for the structural design of bimetallic cocatalysts can be implemented in the future.

Keywords: photocatalysis; solar light degradation; TiO_2 surface grafting; metallic clusters; microwave assisted synthesis

Academic Editors: Jean-François Lamonier and Roberto Fiorenza

Received: 30 December 2024
Revised: 30 May 2025
Accepted: 11 June 2025
Published: 14 June 2025

Citation: Šuligoj, A.; Nadagouda, M.; Žerjav, G.; Pintar, A.; Dionysiou, D.D.; Tušar, N.N. Efficiency of Microwave-Assisted Surface Grafting of Ni and Zn Clusters on TiO_2 as Cocatalysts for Solar Light Degradation of Cyanotoxins. *Catalysts* **2025**, *15*, 590. https://doi.org/10.3390/catal15060590

1. Introduction

Cyanotoxins pose a significant environmental threat globally due to algal blooms, which are becoming increasingly frequent as a result of intensified farming, human pollution, and other sources that lead to eutrophication. For example, the World Health Organization (WHO) has set the concentration limit of the most potent of cyanotoxins microcystin LR (MC-LR) at 1 μg/L [1]. Advanced oxidation processes (AOPs) generate reactive oxygen species (ROS), e.g., hydroxyl ($^{\bullet}OH$), superoxide ($O_2^{\bullet -}$) radicals, and others,

that are responsible for the abatement of the parent molecule and have been used to remedy the MC-LR pollution problem. In this context, titanium dioxide (TiO_2) remains one of the most widely used semiconductors for producing these ROS. Notably, several papers [2–4] describe the successful degradation of MC-LR with titania. Also, the overall toxicity is commonly successfully lowered via TiO_2 photocatalysis [5]. MC-LR binds at three sites of the serine/threonine protein phosphatases: (i) Adda residue interacts with the hydrophobic groove region of PP-1c, (ii) carboxyl group of the MeAsp residue of MC-LR interacts with Arg96 and Tyr134 of PP-1c blocking the access to the active center of the enzyme, and, lastly, (iii) MC-LR coordinates with the two catalytic metal atoms of the phosphatase indirectly by binding two water molecules through the α-carboxyl group of its γ-linked d-glutamic acid moiety. The ability to bind to these sites makes MC-LR the most toxic of cyanotoxins. It also means that attacking the molecule in any way, e.g., by hydroxylation or hydrogen abstraction—phenomena commonly found in the photocatalytic degradation pathways—drastically decreases its toxicity [2,6].

Although plenty research regarding TiO_2 photocatalytic removal of MC-LR has been conducted lately, He et al. have recognized the following three major pitfalls of these systems [2]. Firstly, TiO_2 has a large band gap, utilizing only around 5% of the energy in the solar spectrum. Second is the low quantum efficiency of titania, which is caused by relatively high recombination. Thirdly, the separation and recovery of nano-sized powdered TiO_2 increases the cost of operation dramatically. Hence, more research effort is needed in this area to produce better materials and discover novel ways to remedy this environmental problem. Recently, these efforts have sprung novel types of materials, such as core–shell TiO_2 with NIR-irradiation response, which was used for MC-LR decontamination study [3].

TiO_2 is widely used as a light absorbing semiconductor decorated with metallic (nanoparticles and single atom) and bimetallic cocatalysts [7–9]. However, bimetallic modification requires specific tailoring of the positioning of the cocatalysts on the surface to fully utilize their potential [10]. Modification of the TiO_2 surface with Cu has recently been reported to induce positive effects on photocatalytic performance due to the creation of Cu–O–Ti bonds, through which the recombination of charge carriers is delayed [11,12]. Yet, at higher Cu loadings, i.e., >0.1 mol.% (0.13 wt.%), amorphous Cu(II) oxides are formed, which hinder photocatalytic activity. Other transition metals and certain rare Earth metals have been used in similar approaches to increase the activity under solar light [13,14]. We have shown [15] that activity is hindered at higher loadings of grafted metals on the surface—which is the case for many transition metals—based on the positions of the energy band gaps of the corresponding oxides. Following these research outcomes, we chose nickel and zinc as grafting components due to their appropriate band positions. For instance, Ni was proven to be an effective grafting species due to TiO_2–generated electrons that are transferred to the Ni moieties via the Ti–O–Ni linkage because of the well-matched redox potentials of TiO_2/Ti^{3+} (−0.67 V vs. NHE) with Ni^{2+}/Ni (−0.26 vs. NHE) [16]. Moreover, the redox potentials of $Ni^{2+/0}$ and $Zn^{2+/0}$ are close to the $O_2/O_2^{\bullet-}$ level, which facilitates the reduction of O_2 and hence promotes the cocatalyst activity of such surface clusters [17]. Coincidentally, Ni and Zn also have one of the lowest nobility indices (Z_n) amongst transition metals, meaning they form a stable two-phase equilibria with other compounds in a high degree [18]. Recently, this was corroborated in the activity of Ni-grafted ZnO for the reduction in Cr(VI) and removal of several pharmaceuticals from water [19]. Since $O_2^{\bullet-}$ is the most important ROS under visible irradiation [20], we hypothesize the synthesis of finely dispersed Ni or/and Zn clusters on TiO_2's surface would increase the production of this ROS.

Microwave-assisted (MW) irradiation is a clean, cost-effective, and energy-efficient synthesis procedure that results in high yields in short reaction times [21]; MW has been

shown to improve the size distribution of the grafted nanoparticles (NPs) or clusters and to enhance the structural and morphological properties of nanomaterials [22]. MW-heating could aid the synthesis by enhancing the adsorption of the grafting transition metals. The chloride precursors of Ni and Zn were chosen due to the influence of Cl^- in the MW synthesis since it was shown that Cl^- in the presence of O_2 (dissolved in a solvent) more favorably form 1D, cubic, and bi-pyramid particles, especially with sharp edges [23]. Recently, MW-heating has been applied to anchor carbon [24], C-quantum dots [25] on TiO_2 and to modify its surface with MW-heating to increase Ti^{3+} and Ti–OH content [26,27].

Herein, we provide a method for surface grafting of pre-crystallized TiO_2. We achieve this by introducing nickel or/and zinc chlorides into a water solution to graft the titania's surface with metal clusters and then applying MW irradiation to induce the binding of the metal precursors to the TiO_2's surface, ensuring a monomodal size distribution of the grafted metals. This way we show a low-energy-consumption method and a facile one-pot synthesis of materials that can successfully treat water for detoxification of cyanotoxins with the goal of finding the optimal loading degree. Additionally, bimetal grafting (NiZn) is studied to examine the possible synergism between Ni and Zn clusters on the surface of TiO_2.

2. Results and Discussion

The synthesized catalysts were tested for their visible light photocatalytic degradation of microcystin LR (Figure 1B).

2.1. Photocatalytic Activities

We optimized both the catalyst synthesis and the reaction conditions. The optimization of the former is thoroughly described in the supporting information file (Figure S1A) while the results of the latter are shown in Figure 1C. Here, we present the results of a crucial and often overlooked parameter in immobilized photocatalysis—mechanical stability (Figure S1B).

The sonication test checks both adhesive and cohesive integrity. The highest resistance to mechanical stress in the form of ultrasonic vibration was found for the sample with the lowest amount of n-propanol. The results indicate that curing time is a crucial parameter in the synthesis of coatings. Curing the coatings for one week instead of only one day significantly improved the mechanical stability of the coatings (Figure S1B)—a consequence of the prolonged crosslinking of the Si–O–Si network during the longer aging. The results are similar to those obtained by Kete et al. [28] and Tasbihi et al. [29] whose films lost similar amounts of catalyst exposed to the same treatment. It should be noted that the test is more stringent than the conditions in the reactor. This was confirmed by measuring the detachment after each catalyst test, and no fouling of the catalyst was observed in any of the samples. However, the test is also useful for possible scale-up and other applications where stronger mechanical forces are encountered. Consequently, an optimal amount of solvent (0.5 mL) was chosen for all further immobilizations. The samples were cured in air for one week before being tested in photocatalytic reactions.

The adsorption properties of the coatings were then tested with different TiO_2 particles (Figure S2). Unmodified TiO_2 showed noticeable adsorption within two hours of the reaction, resulting in a removal efficiency of ~38%. The addition of Ni and Zn clusters on the surface did not affect the final degree of removal, and the adsorption–desorption equilibrium was reached within the first 5 min. Thus, the degree of adsorption should not affect the catalytic results of the differently grafted samples. This is to be expected since the amount of grafted species was small (0–1.5 wt.%), and it is unlikely that the grafted species would increase the degree of adsorption; similar results were obtained with 1 wt.%

Fe-grafted TiO_2 [30]. The experimental design (Figure 1A) was then such that the light source was turned on in conjunction with the addition of MC-LR to the system.

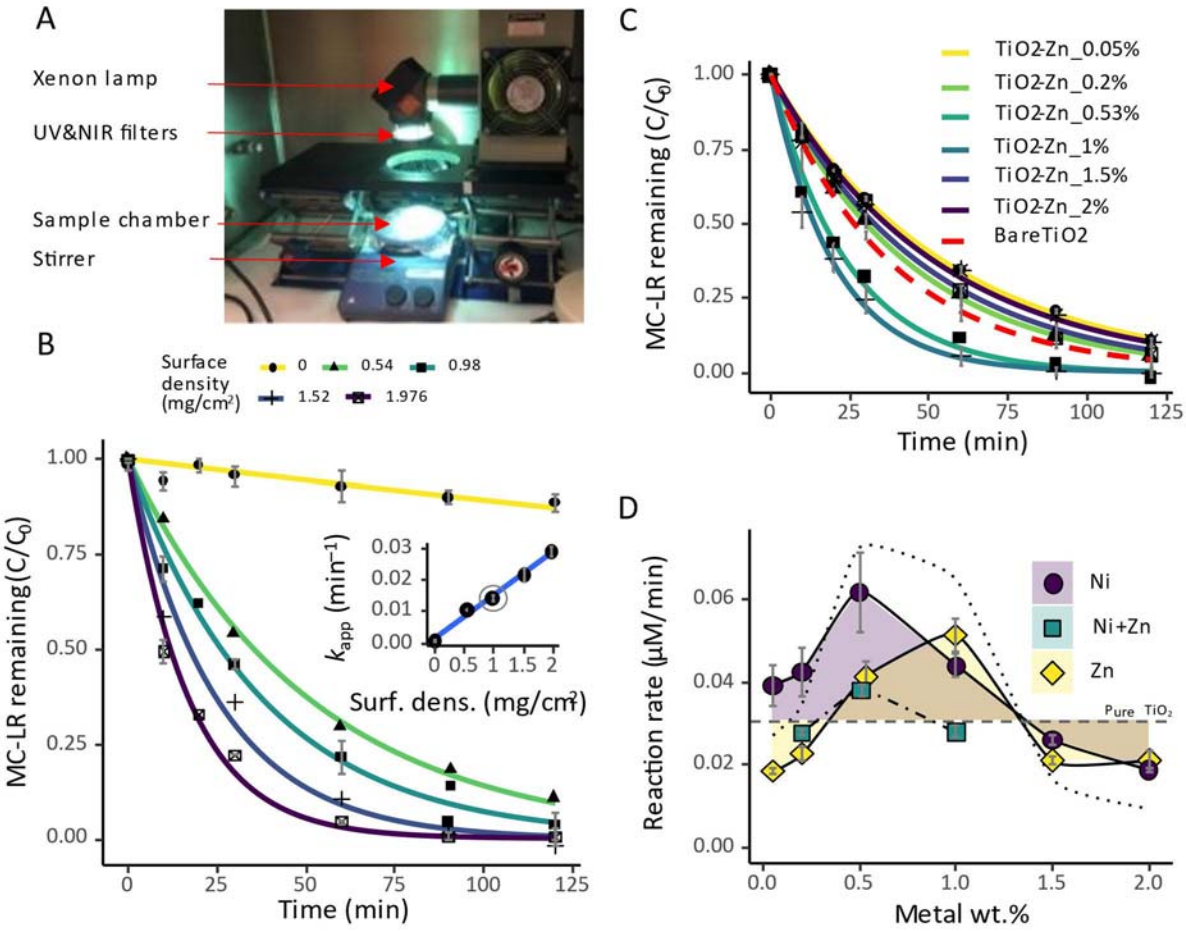

Figure 1. Photocatalytic reactor set-up (**A**), temporal profiles of MC-LR during photocatalytic reactions with samples of different surface densities (**B**). The inset shows the relationship between the apparent first-order reaction rate constant, and the density of the catalyst immobilized on the glass; the chosen surface density for all further tests is marked with a circle. MC-LR removal kinetics with Zn-modified TiO_2 samples (**C**). Dependence of the reaction rates (r) on the nominal loading of nanoclusters of Ni and Zn on the surface of titania (**D**). The dashed gray line represents the level with r of pure TiO_2. The dashed line marks a theoretical summation of rates with the bimetal modification. Error bars represent standard error of the mean (n = 3). Reaction conditions: T = 22 °C, mixing speed = 600 rpm, C_0 = 500 µg/L, P = 500 W, m(cat) = 8.3 mg.

The optimization of catalyst mass, i.e., surface density loading, on reaction kinetics is shown in Figure 1B. As the surface density of pure TiO_2 on the slides increased, the degradation rate of MC-LR increased linearly upon illumination (inset in Figure 1B). This means that in this region, all incoming photons are efficiently absorbed and there are no shadowing, agglomeration, or supersaturation effects. In contrast, in the plateau region, shadowing effects and mass transfer limitations become more important (in our case > 2 mg/cm^2) and hinder further enhancement of the photocatalytic rate. Since it is important to compare the catalysts at their full operating capacity, a surface density of 1.0 mg/cm^2 was chosen. This ensured that the catalysts operated in the linear range with complete absorption of incoming photons and minimal restriction of mass transfer on the catalyst surface. In this way, the grafting of clusters onto the surface of titania can be efficiently studied. If a decrease in activity is observed upon cluster loading, the effects of shadowing, agglomeration, or supersaturation can be ruled out.

We have shown in the past that the grafting of Ni and Zn oxo-species onto the surface of TiO_2 is concentration-dependent [13,15]. In other words, at a certain loading level, the positive effects are the greatest, while further increase in the grafting concentration leads to a decrease in activity, which is due to the shadowing effect, the growth of oxo-clusters, their sintering, and the change in their flexibility in accepting and releasing electrons and their function as cocatalysts [15]. Since no growth of titania NPs and no pore plugging was observed in the grafted samples (see results below), the only plausible candidates for the observed catalytic trends remain a change in IFCT function and a decreased recombination rate of the photogenerated species.

The sole metals Ni and Zn (Figure 1C) showed a maximum reaction rate for the degradation of MC-LR at metal loading of 0.5 and 1.0 wt.%, respectively (Figure 1D), similar to previously reported results for terephthalic acid and resazurin ink degradation [15]. The gap in optimal concentration may be a consequence of the different natures of the clusters. The in-depth analysis of this phenomenon is beyond the scope of this paper. Both transition metals exhibit two-electron transfer. However, the reduction potential of Zn is higher than that of Ni (-0.76 and -0.28 V, respectively) and further from $O_2/O_2^{\bullet-}$. It can be deduced that a higher concentration of Zn species on the surface is required to reach the same population of e^- available for the reduction of O_2, which pushes the optimal concentration to higher values. Interestingly, the drop in activity after reaching the optimum concentration is not as deep for Ni as for Zn. Overall, nickel shows a wider concentration range for optimal function as a cocatalyst than zinc. Surprisingly, Zn modification shows negative effects at low coverage dosages. These cannot be attributed to shadowing or sintering effects as described above. The reasons for this observation remain unsolved at this point and would require additional research.

It is interesting to note that the combination of both metals together shows a much smaller positive effect. The improvements in the bimetallic system are far from being synergistic (dashed line in Figure 1D). In fact, only 0.5 wt.% of the combined clusters enhanced the performance, while other concentrations of bimetallic clusters had a detrimental effect on the activity.

2.2. Morphorogical and Structural Characterization

Several characterization techniques have been used to explain these observations. Scanning Electron Microscopy (SEM) and Transmission Electron Microscopy (TEM) reveal that titanium dioxide nanoparticles (NPs) in the pure TiO_2 samples are uniformly distributed around larger SiO_2 particles (Figure 2i), enabling the efficient use of incident light. Thus, the use of fully hydrolyzed SiO_2 particles in combination with a sol–gel-derived silica mesh that served as a binder allowed the TiO_2 NPs to be uniformly distributed on the surface of the coatings. After grafting transition metal clusters, the structure of the catalysts remained intact, with a relatively homogeneous distribution of the two phases, which were clearly separated (Figure 2i,ii). No clear evidence of metal nanoclusters was seen in the SEM imaging. However, in the TEM microphotographs (Figure 2), a very uniform distribution of metal clusters is seen in all three selected grafted samples, and the clusters do not show aggregation that would lead to clogged pores or impaired light penetration. By using MW irradiation, the size of Ni and Zn clusters were kept as small as possible but still ensured their uniform distribution. The Ni and Zn clusters are also uniformly distributed in the bimetallic modified sample, with no preference for either oxide phase (SiO_2 or TiO_2). Due to the low concentrations of Zn and Ni clusters, quantification by the TEM EELS or EDXS methods was not possible. We performed ICP-OES analysis (Table S2) to confirm the presence of clusters in samples with metal loadings according to their highest photocatalytic activity (see Figure 1D). The data show that the measured concentration

is approximately 2.5 times lower than the nominal value. This can be a consequence of the removal of inadequately bonded clusters through extensive washing during the last steps of catalyst synthesis. However, we notice the consistency in the ratio of measured versus nominal values. XPS analysis showed no changes in the surface composition of the samples, indicating that no detectable Ti^{3+} or oxygen vacancies occurred during TiO_2 grafting (Figures S4 and S5). These can be easily detected by the shift in the Ti 2p and O 1s peaks to higher BE values [30]. Thus, the changes in the observed reaction kinetics can solely be attributed to the presence of Ni and Zn clusters on the surface. In other words, Ti^{3+}, oxygen vacancies, or TiO_2 inter-band states, commonly responsible for the synergistic effects of similar semiconductor systems [30,31], give no contribution to the observed effects since they are not present in the prepared catalysts.

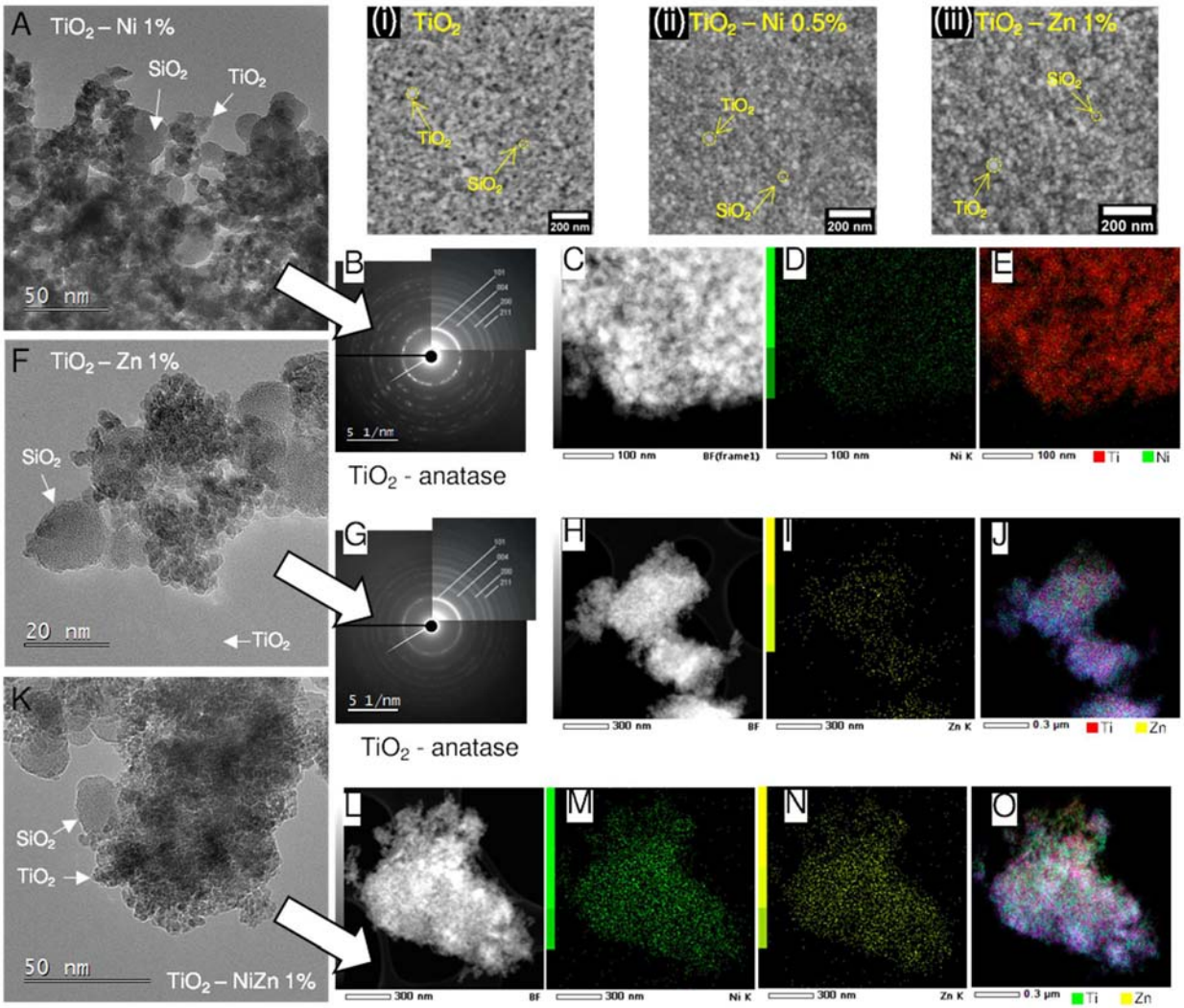

Figure 2. TEM (**A**–**O**) and SEM (**i**–**iii**) images of Ni- (**A**–**E**) and Zn-modified (**F**–**J**) titania samples. Combination of both modification metals is shown in panels (**K**–**O**).

To assess the possible structural changes upon grafting metal clusters onto pristine colloidal TiO_2, samples were studied using nitrogen sorption technique. Isotherms at 77 K show practically identical plateau values below 0.3 P/P_0 value, proving similar specific surface areas (the S_{BET} areas for all samples are in the 320–330 m^2/g range). Furthermore, all the curves exhibit the conventional H2 hysteresis loop, indicating partial obstruction effects within the pore network between the particles. This hysteresis type commonly occurs in the case of a wide distribution of independent pores with the same or similar

neck size or in a network where the neck size distribution is much narrower than the size distribution of the main cavities (e.g., pore-blocking/percolation phenomena play an important role). In our case, the former is a more probable scenario since NPs with homogeneous size distribution were formed, and the degree of aggregation was relatively low (see SEM and TEM images above). Pore sizes calculated from the PSD distribution were slightly increased upon nanocluster loading, i.e., from 8.4 nm for unmodified TiO_2 to 10 nm for 1% Ni-modified TiO_2. This suggests that the space in between the particles increased since the porosity in these materials is intrinsically of interparticle type. It is impossible to reject the hypothesis that the slightly increased pore volume is due to increased interparticle space based on this data; however, no clear proof is given. No intercalation of Ni or Zn atoms inside the TiO_2 lattice was observed using powder XRD (Figure 3C). An analysis of the peak widths at half maxima using the Scherrer equation resulted in crystallite sizes that were all in the range of 8–10 nm, meaning that transition metal grafting did not modify the crystallinity of titania, which is in line with previous reports [15].

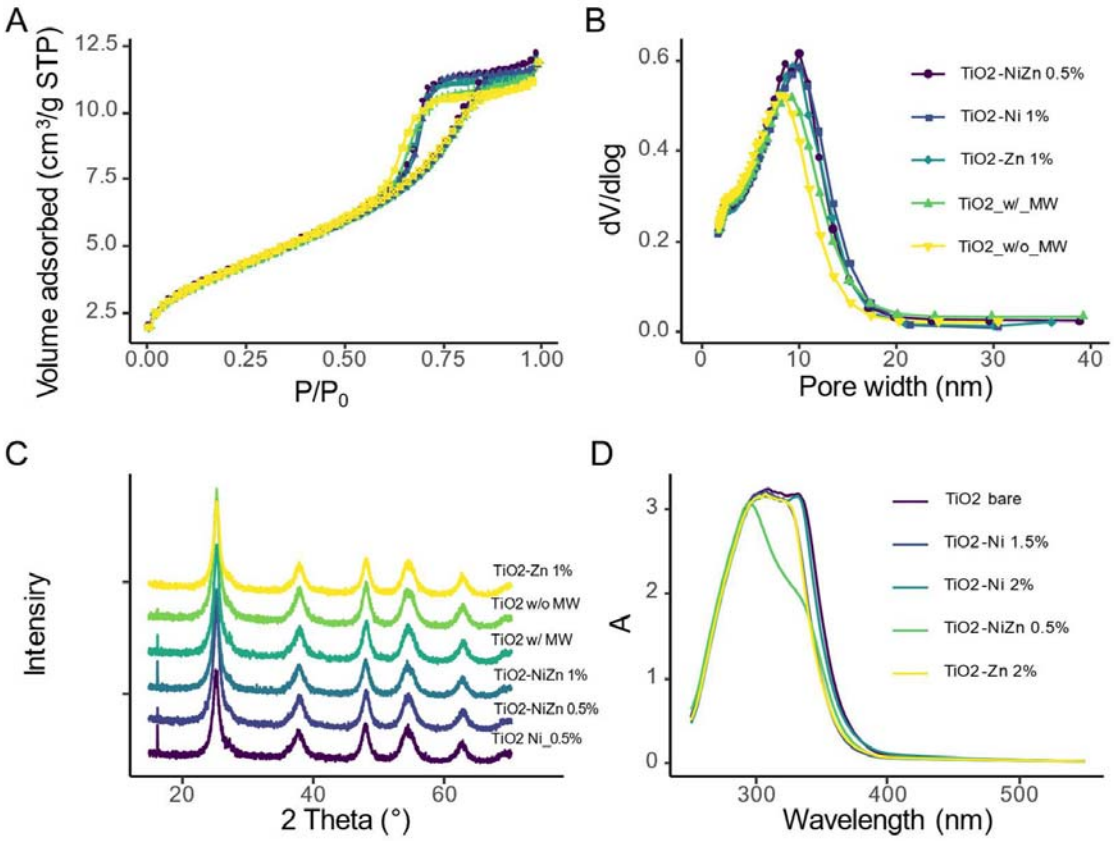

Figure 3. Characterization results of the samples; N_2-sorption isotherms (**A**), the corresponding BJH pore-size distribution (**B**), XRD powder patterns with the major peaks indexed, (**C**) and optical absorption properties of the films (**D**). The color labeling in (**B**) stands for facet (**A**) as well.

Electrical impedance spectroscopy (EIS) and photocurrent measurements were performed to assess the charge transport through the prepared semiconductors. The samples used in this test were loaded with 1 wt.% of metal clusters (Ni, Zn, and NiZn) for better comparison since the bimetallic modification showed a negative contribution to the MC-LR degradation kinetics at this concentration. The electrochemical impedance spectra were analyzed by fitting them to an electrochemical equivalent circuit (EEC; shown as dashed lines in Figure 4A). This model consists of the solution resistance (R_S), the charge transfer resistance (R_{CT}), the Warburg impedance (W), and a constant phase element (CPE) (Figure S7). R_S reflects electrolyte and cell resistance, while R_{CT} is crucial for evaluating

the charge transfer efficiency at the semiconductor/electrolyte interface. The CPE models the non-ideal interfacial capacitance due to surface roughness, and the Warburg element accounts for ion diffusion and carrier transport within the porous photocatalyst layer. Together, these elements provide insight into the charge dynamics that influence photocatalytic activity. A lower R_{CT} value indicates a more efficient charge carrier transfer process, resulting in a longer "lifetime" of the charge carriers. Pure TiO_2 exhibited a high R_{CT} value of 1.263 MΩ. However, the incorporation of Ni and Zn significantly reduced the R_{CT} values, with the TiO_2-Zn sample having the lowest R_{CT} value of 0.258 MΩ among the materials analyzed, which means that the former photocatalyst has a faster electron transfer at the interface along its structure and to the electrode. In the Zn- and Ni-modified samples, the electrons are thus transferred to the surface Zn and Ni clusters, respectively, where they reduce the adsorbed molecules or/and are met with O_2 molecules to further produce $O_2^{\bullet-}$. The lowest e^- transfer resistance in the Zn-modified sample suggests the easiest transfer of electrons, followed by the Ni-modified sample. However, an increase in R_{CT} value in the bimetallic sample suggests poorer interfacial charge transport, namely, more recombination sites—possibly at the interface between the Ni and Zn domains, or at poorly integrated mixed oxide zones. The latter is unlikely due to good distribution of both phases, as evidenced by TEM. However, disruption of established electron pathways is possible: Ni might normally trap e^- effectively while Zn could shift surface properties to enhance hole mobility or adsorption. Together, due to random deposition of binary cocatalysts, they likely create disordered or inhomogeneous energy landscapes that trap both e^- and h^+ inefficiently [10].

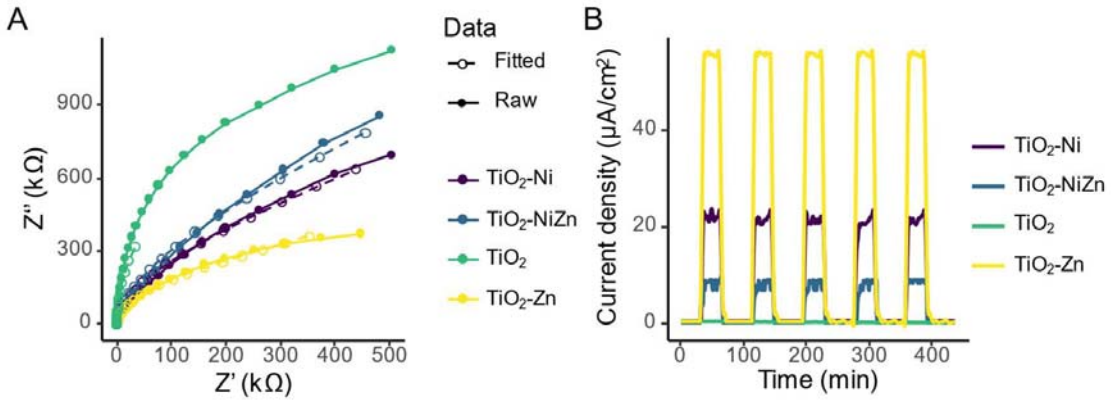

Figure 4. Electrochemical impedance spectra of prepared catalysts (**A**) and photocurrent densities measured under intermittent visible light (Schott, model KL 2500 LED, Mainz, Germany, 410 nm cutoff filter) irradiation in KOH (0.1 M) (**B**). All three modified samples in this series were loaded with 1 wt.% of clusters.

The MC-LR degradation kinetics roughly follow the same trend, i.e., the Zn and Ni modifications with 1 wt.% both show fast degradation kinetics, while the grafting with bimetal NiZn clusters shows the slowest kinetics (Figure 1D).

Similar trends are visible by measuring photocurrent (Figure 4B) under visible light irradiation (λ > 410 nm). The photocurrent intensities followed the trend TiO_2-Zn > TiO_2-Ni > TiO_2-NiZn > TiO_2. This indicates an enhanced photoinduced e^-/h^+ separation, which could be attributed to the synergistic effect of the presence of Ni or Zn clusters at the surface of the TiO_2 semiconductor [32]. Interestingly, the bimetallic modification showed a measurable photocurrent, while bare titania, which exhibited slightly faster kinetics in MC-LR degradation, showed no response. This could imply that (1) the e^-/h^+ separation was increased in all grafted samples while the $O_2^{\bullet-}$ formation was suppressed in the NiZn-modified sample and/or (2) the bimetallic cluster could act as a recombination center on the

surface of the catalyst. The latter would be possible due to the collocation of both Ni and Zn clusters on the surface of titania in NiZn modification (Figure 2O). For example, Benz et al. found [33] that in Pt-loaded TiO_2, in the absence of O_2, after collecting the excited electrons, Pt acts more as a recombination center independent of the amount of Pt deposited.

2.3. Study of Active Species

Since surface clusters of Ni and Zn act as promoters for O_2 reduction [15,19], we investigated the role of reactive oxygen species in the photocatalytic process of MC-LR removal. Previous studies dealing with the visible light TiO_2 photocatalytic degradation of MC-LR showed that $O_2^{\bullet-}$ radicals are the most important reactive species [2,4,20]. In this study, the major reactive oxygen species $^{\bullet}OH$ and $O_2^{\bullet-}$ as well as e_{CB}^-, h_{VB}^+ were thus traced using appropriate quenchers (Figure 5). Although this method only gives a qualitative assessment of the presence of radicals, comparing the materials under the same conditions clearly shows different behavior under the influence of radical scavengers. Most notably, *p*-benzoquinone, an $O_2^{\bullet-}$ scavenger, influenced the bare anatase titania as well as the one modified with 1 wt.% Ni. Additionally, scavenging holes (h^+) also affected the kinetics and final degradation degree of non-modified and Ni-modified samples. Both radical scavengers did not, however, decrease the reaction rate for bimetal modification. In this sample, none of the common quenchers impeded the reaction in a noticeable way.

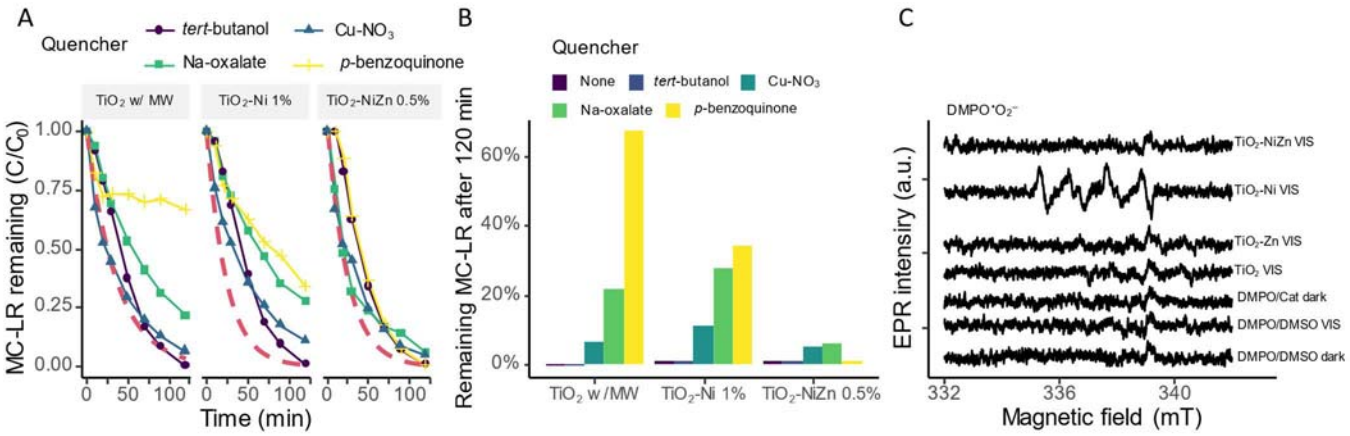

Figure 5. Photocatalytic degradation of microcystin LR in the presence of radical scavengers using different catalysts (**A**,**B**). The red dashed line represents a first-order kinetic fit to an unquenched experiment. The quenchers chosen were *tert*-butanol for $^{\bullet}OH$, 1,4-benzoquinone for $O_2^{\bullet-}$, Cu-nitrate for e^-, and Na-oxalate for h^+. Reaction conditions: C_0 = 500 µg/L, mixing = 600 rpm, T = 23 °C, m(cat) = 8.3 mg. The results of in situ EPR spin trap measurements of DMPO in DMSO (**C**) carried out in the presence of investigated photocatalysts under 15 min visible light exposure (Schott, model KL 2500 LED).

To confirm the generation of superoxide anion radicals ($O_2^{\bullet-}$), DMPO dissolved in DMSO was used to stabilize the DMPO-$O_2^{\bullet-}$ adduct. As can be observed in Figure 5C, both pure DMPO under visible light illumination and DMPO/catalyst suspension in the dark did not produce the characteristic signals of the DMPO-$O_2^{\bullet-}$ adduct (1:1:1:1 quartet). Under 15 min visible light illumination, the bare TiO_2 support and the Zn and NiZn catalysts did not generate a signal for the DMPO-$O_2^{\bullet-}$ adduct (or it was below the detection limit). On the other hand, the Ni/TiO_2 photocatalyst produced $O_2^{\bullet-}$ as the DMPO-$O_2^{\bullet-}$ adduct. Additionally, the broadness of the peaks can be ascribed to the DMPO-OCH_3 adduct formed by the reaction with the solvent (DMSO) under visible light illumination [34] or to the interactions of O_2 with the DMPO-$O_2^{\bullet-}$ adduct [35], as the photocatalyst probably contained small amounts of adsorbed oxygen. The fact that the

Ni-modified sample showed an EPR signal is consistent with the fact that the reduction potential of Zn is higher than that of Ni (−0.76 and −0.28 V, respectively) and further from $O_2/O_2^{\bullet-}$ (−0.33 V) [36].

We notice the occurrence of a delay in the onset of degradation of MC-LR (approx. 10 min, Figure 5A) when using scavengers for $^{\bullet}OH$, 1,4-benzoquinone for $O_2^{\bullet-}$ in the modified samples but not in the bare TiO_2. However, this delay did not appreciably affect the kinetics of MC-LR degradation after this interval. Note that with $Cu(NO_3)$ (e^- scavenger), such a delay in the onset of MC-LR degradation is not seen even though it is known to have a high affinity for adsorption to TiO_2 [20]. For example, Pelaez et al. reported that the adsorption of Cu^{2+} onto TiO_2 decreased the reduction of O_2 by conduction band e^- and partially inhibited the formation of ROS and the removal of MC-LR [20]. A delay step in degradation kinetics is commonly observed with the TiO_2 photocatalytic inactivation of bacteria, where multiple ROS attacks are required before cell membranes are breached [37,38]. In our results, such a phenomenon is unlikely, since it is mostly $O_2^{\bullet-}$ that is responsible for the degradation (EPR data). Hence, *p*-benzoquinone, *tert*-butanol, and Cu-NO_3 may all compete with MC-LR in the consumption of ROS, causing a setback in the degradation of MC-LR. The exact nature of this delay is beyond the scope of this manuscript; it does, however, indicate the presence of competition for adsorption sites as well as the complexity of the degradation mechanism of MC-LR. This could negatively affect the rapid water systems (e.g., rivers and streams) and real aquatic environments where several competing species are present in water. Hence, recyclability and tests with real river water were conducted.

2.4. Recyclability and River Water Test

Reusability of the catalyst is one of the most important traits when considering its practical use. Therefore, two samples, TiO_2-Ni 0.5% and TiO_2-NiZn 0.5%, were subjected to four consecutive runs for degrading MC-LR at the initial concentration of C_0 = 500 µg/L. The samples were cleaned under UV-light (λ_{max} = 365 nm) overnight in between the runs. The results are shown in Figure 6A,B. Both catalysts showed approximately 20% of remaining MC-LR after the second run; the less efficient was the bimetal-modified sample (78% degradation efficiency in the second run). However, they both exhibited regaining of the catalytic activity in the third and fourth reuse cycles, especially TiO_2-Ni 0.5%, which showed a steady increase in the final degradation efficiency. It is worth noting that reaction rate constants increased in the third and fourth reuse cycles and were close to their initial (first run) values after a drop in the second run. This points out that these samples performed well in several reuse cycles for MC-LR degradation.

ATR spectroscopy was used to study the surface of the spent materials (Figure 6D). Fresh bare TiO_2 samples showed the typical band at ~600 cm^{-1}, characteristic for Ti–O–Ti vibration [39], while the absorption at 1100 cm^{-1} is ascribed to Si–O–Si siloxane chains [40,41]. TiO_2-NiZn samples showed characteristic bands at 1360 and 1738 cm^{-1}. These bands can be ascribed to CN stretch and carbonyl bending vibrations, respectively. MC-LR contains C–N moieties in L-Arginine and L-Leucine parts and several carbonyl atoms across the structure. Hence the detection of these suggests the presence of MC-LR leftovers or, more plausible, their degradation products on the surface of the two spent catalysts. Interestingly, these vibrations were not detected in both Ni and Zn single metal-modified samples. This clarifies why the drop in degradation efficiency upon catalyst reuse in the bimetal-modified sample is greater than in the single metal modification. However, even this sample was able to retain its activity upon regeneration with UV irradiation, hence these adsorbed species can be efficiently removed to a large extent via UV regeneration, as has already been reported by others [42].

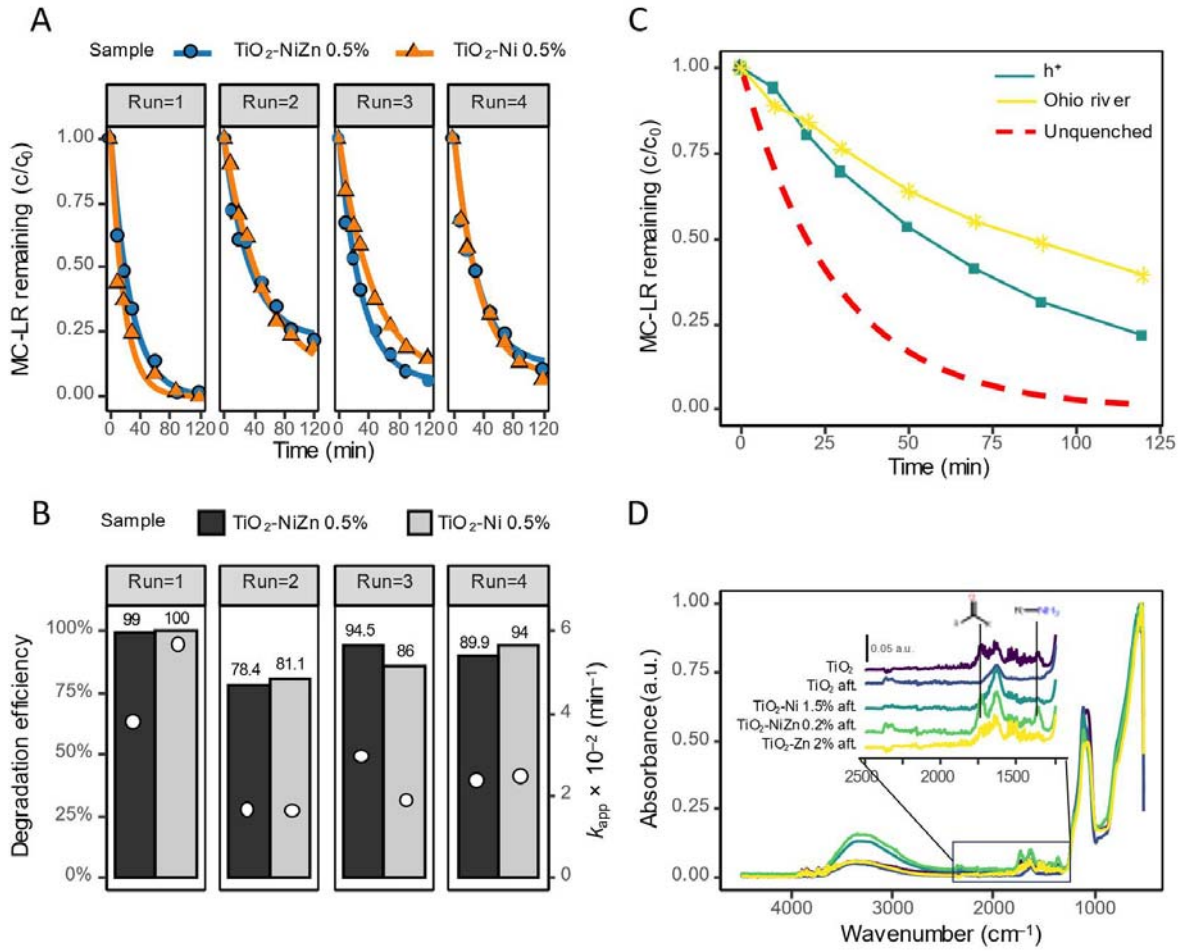

Figure 6. Recycling tests with the use of two catalysts. Kinetic profiles (**A**) and degradation efficiencies (**B**) where ○ represent reaction rate constants (k_{app}) and columns show final degradation efficiencies. Degradation profile of the reaction with real river water with TiO_2-Ni_0.5% (**C**). ATR spectra of fresh (bare TiO_2) and used samples (bare and modified TiO_2_aft. signifies a spent sample) (**D**). The spectra were vertically shifted in the inset in (**D**) for clarity. Reaction conditions: $C_{0(MC\text{-}LR)}$ = 500 µg/L, mixing speed = 600 rpm, T = 23 °C, catalyst dose = 8.3 mg; red dashed line represents an unquenched experiment in deionized water.

The sample was modified with 0.5 wt.% Ni was thus tested for degradation of the Ohio River water spiked with 0.5 mg/mL MC-LR (Figure 6C), where the water was first filtered through a 0.45 cellulose filter to remove the turbidity. The characteristics of the river water on the day of its sampling are given in Table 1, and the exact location is given in the supporting information file (Figure S6). The data show relatively high turbidity, but other than that, other parameters are in the expected range for river water. The results show a much-decreased kinetics of MC-LR degradation—the degradation kinetics is comparable to kinetics as with the use of hole scavenger albeit slightly slower. Although the parameters such as the presence of natural organic matter greatly influence the efficiency of the catalysts, the presence of specific ion species in the water body is of particular interest. It is known that Cl^- act as a hole scavenger in the TiO_2 photocatalytic process [43]. The concentration of Cl^- ions in the river sample (19.5 mg/L) was high enough to support this. Although turbidity was almost completely removed by filtration, this, together with Cl^- ion concentration and slightly higher pH, could be the plausible reasons for the observed performance of the catalyst under these conditions.

Table 1. Measured parameters of the Ohio River at the measurement point (Downtown Cincinnati) on 21 March 2019, which was used in the river water tests of the catalysts.

Parameter	Amount	Unit
Bromide	0.04	mg/L
NO_3	0.91	mg/L
pH	7.8	/
Turbidity	66	NTU
Phosphorus	0.16	mg/L
Chloride	19.5	mg/L
TDS	171	mg/L
PO_4	0.125	mg/L

3. Materials and Methods

3.1. Preparation of Materials

Samples of colloidal TiO_2 nanoparticles (NPs) were kindly donated by Cinkarna, Inc. (commercial name CCA 100 AS, Celje, Slovenia). $NiCl_2.6H_2O$ and $ZnCl_2$ were purchased from Alfa Aesar™ (Stoughton, MA, USA). P-25 (Degussa, Berlin, Germany) C-doped TiO_2 and vlp7000 (Kronos, Leverkusen, Germany) were used as reference photocatalysts. Trifluoroacetic acid (TFA) was purchased from Sigma-Aldrich (Saint Louis, MO, USA). For radical scavenging tests, *tert*-butanol, sodium oxalate, cupric nitrate, and p-benzoquinone were used to scavenge $^{\bullet}OH$, h^+, and $O_2^{\bullet-}$, respectively. Colloidal SiO_2 Levasil 200/30% was purchased from Obermeier (Munich, Germany). TEOS and 1-Propanol were purchased from Sigma-Aldrich (St. Louis, MO, USA). Finally, MC-LR (dry solid, 500 µg) was purchased from Enzo Life Sciences (Farmingdale, NY, USA).

The grafting of titania was carried out in a household microwave oven with a maximum power output of 700 W (EM720CGA.PM, Hamilton Beach Brands, Inc., Glen Allen, VA, USA). The TiO_2 was first diluted to reach a TiO_2 concentration of 1.576 mol/L. To this suspension, appropriate amounts of metal chlorides were added to reach metal nominal percentages of 0.05, 0.2, 0.5, 1, 1.5, and 2 wt.%. The suspensions were first mixed for 1 h at 300 rpm at room temperature, sonicated for 15 min at room temperature, and finally transferred into the microwave and heated at 700 W for 3.5 min. As a reference, previous synthesis involving oil bath at 90 °C required 60 min of heating time to reach adequate grafting of Ni and Zn on the same titania [15]. The method is also comparable to the method for grafting Ni-oxo-clusters on ZnO with an industrial MW reactor [19]. The suspensions were naturally cooled to room temperature and centrifuged at 6000 rpm for 30 min (Sorvall Biofuge Primo from Thermo Fisher, Waltham, MA, USA). The supernatant was discarded, and the tube was refilled with Milli-Q water. The procedure was repeated 3 times to remove residual chlorides.

Such suspension was mixed with a silica binder, which was prepared by mixing TEOS (1.11 mL), Levasil 200/30% (1.7 mL), HCl (32%, 0.03 mL), and isopropanol (5.0 mL). The two suspensions were mixed in a ratio of TiO_2:SiO_2 = 1:2 (v/v), 1-propanol was then added, and the suspension was kept under mixing overnight at room temperature.

The catalysts were then immobilized on glass slides (26 × 35 mm^2) using the doctor-blade technique; 50 µL of suspension was poured over the upper end of the glass and rolled over with a Gardner 4116 Wire-Wound Rod (#16, 30 µm wet thickness; BYK, Geretsried, Germany). After coating, the slides were thermally treated at 150 °C for 10 min. The process was repeated 3–10 times depending on the suspension formulation and the desired mass loading, which were the two parameters of catalyst optimization (Figure 3). Then the slides were activated under UVA-light overnight to remove any organic debris.

3.2. Characterization

Nitrogen sorption measurements were conducted on a Tristar 2000 apparatus (Micromeritics Instrument Corp., Norcross, GA, USA) operating at 77 K; the samples were degassed overnight. The determination of crystal phases present in TiO_2 particles was carried out on 3DXPERT-PRO with Cu-$K_{\alpha 1}$ wavelength of 0.154 nm.

X-ray photoelectron spectroscopy (XPS) analysis was performed on a PHI-TFA XPS spectrometer (Physical Electronics Inc., Chanhassen, MN, USA). The samples were excited by X-ray radiation from a monochromatic Al-Kα source (1468.6 eV). The high-energy-resolution spectra were acquired with an energy analyzer operating at a resolution of about 0.6 eV and a pass energy of 29 eV. During data processing, the C 1s peak at 285.0 eV was used as the reference.

Elemental quantification of metal clusters was recorded in the degradation system by inductively coupled plasma–optical emission spectrometry (ICP-OES, model 715-ES, Varian, Palo Alto, CA, USA).

Autolab PGSTAT30 potentiostat/galvanostat (Metrohm, Herisau, Switzerland) and a three-electrode electrochemical cell were used to evaluate the photo-response characteristics of prepared materials under intermittent visible light illumination (LED SCHOTT KL 1600 lamp (λ_{max} = 450 nm), Mainz, Germany) with 0 V bias potential (vs. SCE). The electrolyte was an aqueous solution of KOH (0.1 M). Then 10 µL of catalyst-ethanol suspension (12.5 mg of catalyst in 2.5 mL of absolute ethanol (Sigma Aldrich)) was dropped onto the surface of the screen-printed DropSens electrode (model DRP-150, Metrohm, Herisau, Switzerland). This presented the working electrode. A calomel electrode (model HI5412, Hanna Instruments S.R.L., Woonsocket, RI, USA) was used as a reference electrode and platinum electrode as a counter electrode.

Electrochemical impedance (EIS) spectra of prepared catalysts were obtained in the frequency range of 0.1–10^6 Hz; 0.1 M KOH was used as the electrolyte. Also, in this case, screen-printed DropSens electrode (DropSens DRP-150, Oviedo, Spain) was used as a working electrode, platinum as a counter electrode, and Ag as a reference electrode.

3.3. Photocatalytic Activity Tests

The photocatalytic activity tests were conducted using a top-down irradiated reactor consisting of a Petri dish (⌀ = 100 mm, height = 30 mm) with a magnetic stirrer bar positioned slightly off center beside the catalyst glass plate (stirring rate = 600 rpm). The reaction was commenced when 20 µL MC-LR (concentration of the stock solution was 250 mg/L) was injected into the reactor filled with 10 mL dH_2O. It should be noted that dark adsorption kinetics were measured in a separate experiment and shown to be finished in 5 min independent of sample modification. Adsorption tests were conducted separately and showed that samples adsorbed ~5% of initial MC-LR (Figure S1), hence the reactions were carried out by turning on irradiation immediately after injecting the MC-LR. The irradiation was provided with a solar simulator (Newport, Irvine, CA, USA) housing a Xenon light (P = 500 W m^{-2}) at a distance of 15 cm from reaction solution at room temperature (22 °C, cooling provided with an air fan). Two light correction filters FSQ-GG420 and FSQ-KG5 (Newport, Irvine, CA, USA) were used to omit UV and IR part of the Xe-lamp irradiation, respectively.

3.4. Analytical Procedures

The quantification of MC-LR was conducted on an Agilent chromatograph using a column Discovery® HS C18 (150 mm × 4.6 mm ID, 5 µm) from Supelco (Bellefonte, PA, USA). An isocratic method consisted of 45% mobile phase A and 55% of mobile phase

B, where A is 0.5% TFA in acetonitrile is and B is 0.5% TFA in water, with the flow of 0.7 mL/min.

To determine the tendency for $O_2^{\bullet -}$ generation, spin trapping experiments were performed with DMPO (5-5-dimethyl-1-pyrroline-N-oxide, ≥98.0%, Sigma Aldrich) dissolved in dimethyl sulfoxide (DMSO, ≥99.9%, Sigma Aldrich) as a solvent. Measurements of the corresponding spin adduct (DMPO-$O_2^{\bullet -}$) were performed at T = 25 °C using a 100 µL liquid flat cell (Fluorochem, Glossop, UK, model WG-808_Q) and an X-band Adani CMS8400 EPR spectrometer (Minsk, Belarus). The illumination source for the visible light in all cases was the Schott KL 2500 LED lamp (Mainz, Germany). The center field was at 337.00 mT (sweep width 10 mT) with a modulation amplitude of 200 µT and a power attenuation of 15 dB (gain value of 4×10^3). The initial concentration of DMPO was 4 g/L and that of the catalyst 2 g/L. The DMSO/catalyst suspension was stirred vigorously (300 rpm) and purged with air (100 mL/min) for 15 min before being used to form the DMPO/DMSO/catalyst suspension and filled into the 100 µL liquid flat cell for in situ measurements.

4. Conclusions

Microwave-synthesized surface-grafted TiO_2 films were shown to be promising material for detoxification of water polluted with cyanotoxin microcystin LR. The grafting using MW was efficient and 17× quicker than the previous heating method [15], and produced uniformly dispersed sub-nano-sized clusters; the films were of excellent mechanical stability. The main species responsible for visible light activity via the interface charge transfer (IFCT) of excited e^- to surface metal clusters were found to be $O_2^{\bullet -}$ and h^+; the former were confirmed with EPR study.

The optimal nominal grafting concentration was 0.5 wt.% for Ni and 1.0 wt.% for Zn, while for the binary modification (NiZn), the optimal nominal concentration was 0.5 wt.%. The efficiency was highly sensitive to the concentration of the grafted species; hence, caution is required during the synthesis as low loadings are required for the desired effect. No synergism with the simultaneous presence of two metals was observed. In fact, compared to single metal grafted TiO_2, the bimetallic clusters (Ni and Zn) on the surface of titania showed decreased photocurrent and increased recombination rate under the visible light irradiation, due poorer interfacial charge transport, resulting in more recombination sites. Nevertheless, the catalysts were easily regenerated using UV irradiation for long-term use. To implement the activity of bimetallic samples in the future, one would want an ideal scenario where Ni acts as reduction cocatalyst while Zn promotes h^+ transfer or adsorption of oxidizable species. For this, we would use spatially controlled deposition, e.g., via sequential grafting (Ni first, then Zn—or vice versa), core–shell structures, where one metal forms a shell over another, or site-selective anchoring on different crystal facets (e.g., Ni on {101}, Zn on {001}). All of these strategies can be achieved efficiently with the help of MW irradiation.

Supplementary Materials: The following supporting information can be downloaded at: https://www.mdpi.com/article/10.3390/catal15060590/s1. Figure S1: Correlation between the number of layers and the surface density using different formulations for the preparation of films (A) and ultrasonic mechanical stability test for samples of AS TiO_2 with different amounts of final solvent (n-propanol) (B). The inset photographs show the layers after enduring the specified sonication time. In the sample "1 mL old", the word old stands for a sample that has been aged in the dark for one week. Figure S2: Adsorption kinetics of various films at 1 mg/cm^2 mass loading. Figure S3: The results of Rietveld refinement of the samples: (a) TiO_2 w/o MW; (b) TiO_2 w/MW; (c) TiO_2_Ni_0.5%; and (d) TiO_2_Zn_1%; with x- and y-axis showing 2 Θ (°) and intensity, respectively. The positions of the Bragg reflections of anatase (structure shown in the inset of A) are indicated by vertical bars (|). The difference curves between the experimental and the calculated intensities from the refined model are shown in the lower part of the diagrams. Figure S4: XPS survey of samples: (a) TiO_2 w/o MW, (b)

TiO_2 w/MW, (c) TiO_2-Ni 1%, (d) TiO_2-Zn 1%, (i) Ti2p, (ii) O1s, and (iii) C1s spectra. Figure S5: XPS survey of the samples (a) TiO_2 w/o MW, (b) TiO_2 w/MW, (c) TiO_2-Ni 1%, (d) TiO_2-Zn 1%, (i) Ti2p, (ii) O1s, and (iii) C1s spectra. Figure S6: Location of the river sample at 13.00 on 21 March 2019. Table S1: Crystallographic data and results of Rietveld refinement of XRD data of TiO_2 samples. Figure S7. Scheme of electrochemical equivalent circuit model used to fit experimental impedance data. Figure S8. Location of river sample at 13.00 on 21 March 2019. Table S2: Elemental composition of selected samples as measured by ICP-OES. Results are shown in weight percent (wt.%).

Author Contributions: A.Š.; Conceptualization, Investigation, Methodology, Formal Analysis, Writing—Original Draft, Funding Acquisition. M.N.; Methodology, Formal Analysis, Writing—Review and Editing. G.Ž.; Formal Analysis, Investigation, Writing—Original Draft. A.P.; Formal Analysis, Investigation, Writing—Review and Editing, Funding Acquisition. D.D.D.; Supervision, Writing—Review and Editing. N.N.T.; Writing—Review and Editing, Project Administration, Funding Acquisition. Author D.D.D. passed away prior to the publication of this manuscript. All authors have read and agreed to the published version of the manuscript.

Funding: Andraž Šuligoj gratefully acknowledges financial support for this publication by the Fulbright U.S. Student Program (2018–2019), which is sponsored by the U.S. Department of State and U.S. Embassy Ljubljana. This research work was also supported by the Slovenian Research and Innovation Agency research programs P1-0418, P2-0150, P1-0134, research projects J2-4444, J1-2472 and NETPORE COST action CA20126.

Data Availability Statement: All data is available in the main text or the Supplementary Materials.

Acknowledgments: Nitrogen physisorption measurements were conducted by Mojca Opresnik and the XRD measurements by Edi Kranjc, both from the National Institute of Chemistry, Ljubljana, for which we are very grateful.

Conflicts of Interest: The authors declare no competing interests.

References

1. WHO. *Guidelines for Drinking Water Quality*, 2nd ed.; Health Criteria and Other Supporting Information; WHO: Geneva, Switzerland, 1998.
2. He, X.; Wang, A.; Wu, P.; Tang, S.; Zhang, Y.; Li, L.; Ding, P. Photocatalytic Degradation of Microcystin-LR by Modified TiO_2 Photocatalysis: A Review. *Sci. Total Environ.* **2020**, *743*, 140694. [CrossRef]
3. Wu, S.; Lv, J.; Wang, F.; Duan, N.; Li, Q.; Wang, Z. Photocatalytic Degradation of Microcystin-LR with a Nanostructured Photocatalyst Based on Upconversion nanoparticles@TiO_2 Composite under Simulated Solar Lights. *Sci. Rep.* **2017**, *7*, 14435. [CrossRef]
4. Fotiou, T.; Triantis, T.M.; Kaloudis, T.; O'Shea, K.E.; Dionysiou, D.D.; Hiskia, A. Assessment of the Roles of Reactive Oxygen Species in the UV and Visible Light Photocatalytic Degradation of Cyanotoxins and Water Taste and Odor Compounds Using C-TiO_2. *Water Res.* **2016**, *90*, 52–61. [CrossRef]
5. Campos, A.; Vasconcelos, V. Molecular Mechanisms of Microcystin Toxicity in Animal Cells. *Int. J. Mol. Sci.* **2010**, *11*, 268–287. [CrossRef]
6. Chintalapati, P.; Mohseni, M. Degradation of Cyanotoxin Microcystin-LR in Synthetic and Natural Waters by Chemical-Free UV/VUV Radiation. *J. Hazard. Mater.* **2020**, *381*, 120921. [CrossRef]
7. Kerketta, U.; Tesler, A.B.; Schmuki, P. Single-Atom Co-Catalysts Employed in Titanium Dioxide Photocatalysis. *Catalysts* **2022**, *12*, 1223. [CrossRef]
8. Zaera, F. Role of Metal Cocatalysts in the Photocatalytic Production of Hydrogen from Water Revisited. *Energy Fuels* **2025**, *39*, 2422–2434. [CrossRef]
9. Šuligoj, A.; Cerc Korošec, R.; Žerjav, G.; Novak Tušar, N.; Lavrenčič Štangar, U. Solar-Driven Photocatalytic Films: Synthesis Approaches, Factors Affecting Environmental Activity, and Characterization Features. *Top. Curr. Chem.* **2022**, *380*, 51. [CrossRef]
10. Meng, A.; Zhang, L.; Cheng, B.; Yu, J. Dual Cocatalysts in TiO_2 Photocatalysis. *Adv. Mater.* **2019**, *31*, 1807660. [CrossRef]
11. Čižmar, T.; Lavrenčič Štangar, U.; Fanetti, M.; Arčon, I. Effects of Different Copper Loadings on the Photocatalytic Activity of TiO_2-SiO_2 Prepared at a Low Temperature for the Oxidation of Organic Pollutants in Water. *ChemCatChem* **2018**, *10*, 2982–2993. [CrossRef]
12. Pozan, G.S.; Isleyen, M.; Gokcen, S. Transition Metal Coated TiO_2 Nanoparticles: Synthesis, Characterization and Their Photocatalytic Activity. *Appl. Catal. B Environ.* **2013**, *140–141*, 537–545. [CrossRef]

13. Toledo-Antonio, J.A.; Piccirillo, C.; Rozman, N.; Pullar, R.C.; Seabra, M.P.; Škapin, A.S.; Castro, P.M.L.; Labrincha, J.A. Effects of Cu, Zn and Cu-Zn Addition on the Microstructure and Antibacterial and Photocatalytic Functional Properties of Cu-Zn Modified TiO_2 Nano-Heterostructures. *J. Photochem. Photobiol. A Chem.* **2016**, *330*, 44–54. [CrossRef]
14. Pliekhova, O.; Arčon, I.; Pliekhov, O.; Tušar, N.N.; Štangar, U.L. Cu and Zr Surface Sites in the Photocatalytic Activity of TiO_2 Nanoparticles. *Environ. Sci. Pollut. Res.* **2017**, *24*, 12571–12581. [CrossRef]
15. Šuligoj, A.; Arčon, I.; Mazaj, M.; Dražić, G.; Arčon, D.; Cool, P.; Štangar, U.L.; Tušar, N.N. Surface Modified Titanium Dioxide Using Transition Metals: Nickel as a Winning Transition Metal for Solar Light Photocatalysis. *J. Mater. Chem. A* **2018**, *6*, 9882–9892. [CrossRef]
16. Fan, L.; Long, J.; Gu, Q.; Huang, H.; Lin, H.; Wang, X. Single-Site Nickel-Grafted Anatase TiO_2 for Hydrogen Production: Toward Understanding the Nature of Visible-Light Photocatalysis. *J. Catal.* **2014**, *320*, 147–159. [CrossRef]
17. Nussbaum, M.; Shaham-Waldmann, N.; Paz, Y. Synergistic Photocatalytic Effect in Fe,Nb-Doped BiOCl. *J. Photochem. Photobiol. A Chem.* **2014**, *290*, 11–21. [CrossRef]
18. Hegde, V.I.; Aykol, M.; Kirklin, S.; Wolverton, C. The Phase Stability Network of All Inorganic Materials. *Sci. Adv.* **2020**, *6*, eaay5606. [CrossRef]
19. Ravbar, M.; Maver, K.; Knaflič, T.; Arčon, I.; Novak Tušar, N.; Lavrenčič Štangar, U.; Šuligoj, A. Nickel-Decorated ZnO Nanoparticles for Effective Solar Reduction of Hexavalent Chromium and Removal of Selected Pharmaceuticals. *Appl. Surf. Sci.* **2025**, *681*, 161463. [CrossRef]
20. Pelaez, M.; Falaras, P.; Likodimos, V.; O'Shea, K.; de la Cruz, A.A.; Dunlop, P.S.M.; Byrne, J.A.; Dionysiou, D.D. Use of Selected Scavengers for the Determination of NF-TiO_2 Reactive Oxygen Species during the Degradation of Microcystin-LR under Visible Light Irradiation. *J. Mol. Catal. A Chem.* **2016**, *425*, 183–189. [CrossRef]
21. Baghbanzadeh, M.; Carbone, L.; Cozzoli, P.D.; Kappe, C.O. Microwave-Assisted Synthesis of Colloidal Inorganic Nanocrystals. *Angew. Chem. Int. Ed.* **2011**, *50*, 11312–11359. [CrossRef]
22. Tu, W.; Liu, H. Rapid Synthesis of Nanoscale Colloidal Metal Clusters by Microwave Irradiation. *J. Mater. Chem.* **2000**, *10*, 2207–2211. [CrossRef]
23. Tsuji, M.; Matsumoto, K.; Jiang, P.; Matsuo, R.; Tang, X.L.; Kamarudin, K.S.N. Roles of Pt Seeds and Chloride Anions in the Preparation of Silver Nanorods and Nanowires by Microwave-Polyol Method. *Colloids Surf. A Physicochem. Eng. Asp.* **2008**, *316*, 266–277. [CrossRef]
24. Oseghe, E.O.; Ofomaja, A.E. Facile Microwave Synthesis of Pine Cone Derived C-Doped TiO_2 for the Photodegradation of Tetracycline Hydrochloride under Visible-LED Light. *J. Environ. Manag.* **2018**, *223*, 860–867. [CrossRef]
25. Li, M.; Wang, M.; Zhu, L.; Li, Y.; Yan, Z.; Shen, Z.; Cao, X. Facile Microwave Assisted Synthesis of N-Rich Carbon Quantum Dots/Dual-Phase TiO_2 Heterostructured Nanocomposites with High Activity in CO_2 Photoreduction. *Appl. Catal. B Environ.* **2018**, *231*, 269–276. [CrossRef]
26. Han, E.; Vijayarangamuthu, K.; Youn, J.; Park, Y.-K.; Jung, S.-C.; Jeon, K.-J. Degussa P25 TiO_2 Modified with H_2O_2 under Microwave Treatment to Enhance Photocatalytic Properties. *Catal. Today* **2018**, *303*, 305–312. [CrossRef]
27. Zhang, Z.; Yang, X.; Hedhili, M.N.; Ahmed, E.; Shi, L.; Wang, P. Microwave-Assisted Self-Doping of TiO_2 Photonic Crystals for Efficient Photoelectrochemical Water Splitting. *ACS Appl. Mater. Interfaces* **2014**, *6*, 691–696. [CrossRef]
28. Kete, M.; Pavlica, E.; Fresno, F.; Bratina, G.; Štangar, U.L. Highly Active Photocatalytic Coatings Prepared by a Low-Temperature Method. *Environ. Sci. Pollut. Res.* **2014**, *21*, 11238–11249. [CrossRef]
29. Tasbihi, M.; Călin, I.; Šuligoj, A.; Fanetti, M.; Lavrenčič Štangar, U. Photocatalytic Degradation of Gaseous Toluene by Using TiO_2 Nanoparticles Immobilized on Fiberglass Cloth. *J. Photochem. Photobiol. A Chem.* **2017**, *336*, 89–97. [CrossRef]
30. Kong, L.; Wang, C.; Wan, F.; Zheng, H.; Zhang, X. Synergistic Effect of Surface Self-Doping and Fe Species-Grafting for Enhanced Photocatalytic Activity of TiO_2 under Visible-Light. *Appl. Surf. Sci.* **2017**, *396*, 26–35. [CrossRef]
31. Balayeva, N.O.; Fleisch, M.; Bahnemann, D.W. Surface-Grafted WO_3/TiO_2 Photocatalysts: Enhanced Visible-Light Activity towards Indoor Air Purification. *Catal. Today* **2018**, *313*, 63–71. [CrossRef]
32. Zhang, M.; Xiong, J.; Yang, H.; Wen, Z.; Chen, R.; Cheng, G. Surface Potential/Wettability and Interface Charge Transfer Engineering of Copper-Oxide (Cu–MOx, M = W, Ti, and Ce) Hybrids for Efficient Wastewater Treatment through Adsorption–Photocatalysis Synergy. *Ind. Eng. Chem. Res.* **2020**, *59*, 15454–15463. [CrossRef]
33. Benz, D.; Felter, K.M.; Köser, J.; Thöming, J.; Mul, G.; Grozema, F.C.; Hintzen, H.T.; Kreutzer, M.T.; Van Ommen, J.R. Assessing the Role of Pt Clusters on TiO_2 (P25) on the Photocatalytic Degradation of Acid Blue 9 and Rhodamine B. *J. Phys. Chem. C* **2020**, *124*, 8269–8278. [CrossRef]
34. Dvoranová, D.; Barbieriková, Z.; Brezová, V. Radical Intermediates in Photoinduced Reactions on TiO_2 (An EPR Spin Trapping Study). *Molecules* **2014**, *19*, 17279–17304. [CrossRef]
35. Khachatryan, L.; Vejerano, E.; Lomnicki, S.; Dellinger, B. Environmentally Persistent Free Radicals (EPFRs). 1. Generation of Reactive Oxygen Species in Aqueous Solutions. *Environ. Sci. Technol.* **2011**, *45*, 8559–8566. [CrossRef]
36. Wood, P.M. The Potential Diagram for Oxygen at pH 7. *Biochem. J.* **1988**, *253*, 287–289. [CrossRef]

37. Chang, C.-W.; Huo, X.; Lin, T.-F. Exposure of Microcystis Aeruginosa to Hydrogen Peroxide and Titanium Dioxide under Visible Light Conditions: Modeling the Impact of Hydrogen Peroxide and Hydroxyl Radical on Cell Rupture and Microcystin Degradation. *Water Res.* **2018**, *141*, 217–226. [CrossRef]
38. Ateia, M.; Alalm, M.G.; Awfa, D.; Johnson, M.S.; Yoshimura, C. Modeling the Degradation and Disinfection of Water Pollutants by Photocatalysts and Composites: A Critical Review. *Sci. Total Environ.* **2020**, *698*, 134197. [CrossRef]
39. Šuligoj, A.; Lavrenčič Štangar, U.; Novak Tušar, N. Photocatalytic Air-Cleaning Using TiO_2 Nanoparticles in Porous Silica Substrate. *Chem. Pap.* **2014**, *68*, 1265–1272. [CrossRef]
40. Launer, P.J. Infrared Analysis of Organosilicon Compounds: Spectra-Structure Correlations. In *Silicon Compounds: Register and Review*; Petrarch Systems: Bristol, PA, USA, 1987; pp. 100–103.
41. Maučec, D.; Šuligoj, A.; Ristić, A.; Dražić, G.; Pintar, A.; Tušar, N.N. Titania versus Zinc Oxide Nanoparticles on Mesoporous Silica Supports as Photocatalysts for Removal of Dyes from Wastewater at Neutral pH. *Catal. Today* **2018**, *310*, 32–41. [CrossRef]
42. Pichat, P. *Photocatalysis and Water Purification: From Fundamentals to Recent Applications*, 1st ed.; Pichat, P., Ed.; Wiley-VCH Verlag GmbH & Co. KGaA: Weinheim, Germany, 2013; ISBN 9783527329878.
43. Iguchi, S.; Teramura, K.; Hosokawa, S.; Tanaka, T. Effect of the Chloride Ion as a Hole Scavenger on the Photocatalytic Conversion of CO_2 in an Aqueous Solution over Ni–Al Layered Double Hydroxides. *Phys. Chem. Chem. Phys.* **2015**, *17*, 17995–18003. [CrossRef]